nature chemistry

ARTICLES

PUBLISHED ONLINE: 23 MARCH 2015 | DOI: 10.1038/NCHEM.2203

An aptamer-functionalized chemomechanically modulated biomolecule catch-and-release system

Ankita Shastri[1], Lynn M. McGregor[1], Ya Liu[2], Valerie Harris[3], Hanqing Nan[4], Maritza Mujica[4], Yolanda Vasquez[1,5†], Amitabh Bhattacharya[2†], Yongting Ma[2†], Michael Aizenberg[6], Olga Kuksenok[2], Anna C. Balazs[2], Joanna Aizenberg[1,5,6,7*] and Ximin He[3,4,5*]

The efficient extraction of (bio)molecules from fluid mixtures is vital for applications ranging from target characterization in (bio)chemistry to environmental analysis and biomedical diagnostics. Inspired by biological processes that seamlessly synchronize the capture, transport and release of biomolecules, we designed a robust chemomechanical sorting system capable of the concerted catch and release of target biomolecules from a solution mixture. The hybrid system is composed of target-specific, reversible binding sites attached to microscopic fins embedded in a responsive hydrogel that moves the cargo between two chemically distinct environments. To demonstrate the utility of the system, we focus on the effective separation of thrombin by synchronizing the pH-dependent binding strength of a thrombin-specific aptamer with volume changes of the pH-responsive hydrogel in a biphasic microfluidic regime, and show a non-destructive separation that has a quantitative sorting efficiency, as well as the system's stability and amenability to multiple solution recycling.

Numerous biological processes involve the synchronized trapping, transporting and sorting of specific biomolecules within complex fluids[1]. These processes arise from a chemomechanically modulated inherent integration of molecular recognition, reconfiguration and micromechanical motion of components in response to various internal signals[1,2]. In contrast, several current techniques for biomolecule sorting often require significant, and sometimes disruptive, biomolecule modification, many sequential steps and a high energy input from lasers and sources of electrical fields, infrared radiation or magnetic fields[3–8]. Although some methods (for example, those that involve magnetic beads[9]) show an efficient capture of biomolecules without substantial alteration of the target, controllable continuous separation and transfer between solutions *in situ* can be achieved by combining complementary responsive materials, which also permit the system to be tailored to meet the requirements of different applications. Recently, considerable effort has been devoted to developing dynamic micro- and nanoscale hybrid systems that exploit the precise geometry of their components, combine chemical and mechanical action, act in a multimodal fashion and even generate autonomous movement or autoregulation[10–19]. Such dynamic chemomechanical approaches, if applied to biomolecule detection and separation, could advance chemical and clinical technologies that focus on diagnostics and purification.

Here we draw inspiration from the ability of vesicle-carrying kinesins and dyneins to shuttle different biomolecule cargoes along the microtubule network[20] to develop a conceptually new chemomechanobiochemically modulated system that performs a sequential, self-regulated 'catch–transport–release' of target biomolecules from one fluid flow to another. Critical components for our cooperative hierarchical system include: (1) compartments that provide two chemically distinct environments, (2) a stimuli-responsive affinity handle for the biomolecules that can bind the target in one environment and release it in another, (3) a dynamic 'arm' that moves the cargo between the two compartments and (4) an 'artificial muscle' that actuates the arm's motion.

In our system, the chemically distinct environments are produced via a microfluidic system that yields two parallel fluid streams undergoing laminar flow. Aptamers (short DNA, RNA or peptide molecules that recognize specific chemical targets) serve as the stimuli-responsive affinity handles because of their ability to bind target molecules reversibly in different environments[21,22] (for example, DNA aptamers can denature and refold to capture and release their targets in response to temperature or pH changes). The dynamic arms are supplied by aptamer-decorated, polymeric microscopic fins that are embedded in a stimuli-responsive hydrogel, which undergoes significant volumetric changes in response to environmental cues and, thus, functions as the actuating 'muscle' that drives the reversible bending of microstructures[23–25]. Importantly, the reversible aptamer folding and biomolecule binding are synchronized with the reversible volume changes of the hydrogels such that the polymeric microfins provide a coordinated transportation of cargo between the compartments in the microfluidic system and result in the efficient capture and separation of biomolecules. This design is distinct from conventional biomolecule-sorting systems by its reliance on a concerted cascade of chemomechanobiochemical energy transduction, as opposed to isolated energy inputs in the form of laser, electrical or magnetic fields.

An especially useful feature of this system is that the hydrogel and aptamer binding can be chosen to respond to the same

[1]Department of Chemistry and Chemical Biology, Harvard University, Cambridge, Massachusetts 02138, USA. [2]Department of Chemical and Petroleum Engineering, University of Pittsburgh, Pittsburgh, Pennsylvania 15261, USA. [3]Center for Molecular Design and Biomimetics, The Biodesign Institute, Arizona State University, Tempe, Arizona 85287, USA. [4]Materials Science and Engineering, School for Engineering of Matter, Transport and Energy, Arizona State University, Tempe, Arizona 85287, USA. [5]School of Engineering and Applied Science, Harvard University, Cambridge, Massachusetts 02138, USA. [6]Wyss Institute for Biologically Inspired Engineering, Harvard University, Cambridge, Massachusetts 02138, USA. [7]Kavli Institute for Bionano Science and Technology, Harvard University, Cambridge, Massachusetts 02138, USA. [†]Present address: Department of Chemistry, Oklahoma State University, Stillwater, Oklahoma 74078, USA (Y.V.). Department of Mechanical Engineering, Indian Institute of Technology Bombay, Powai, Maharastra 400 076, India (A.B.). Department of Chemical Engineering, Louisiana State University, Baton Rouge, Louisiana 70803, USA (Y.M.). *e-mail: jaiz@seas.harvard.edu; ximin.he@asu.edu

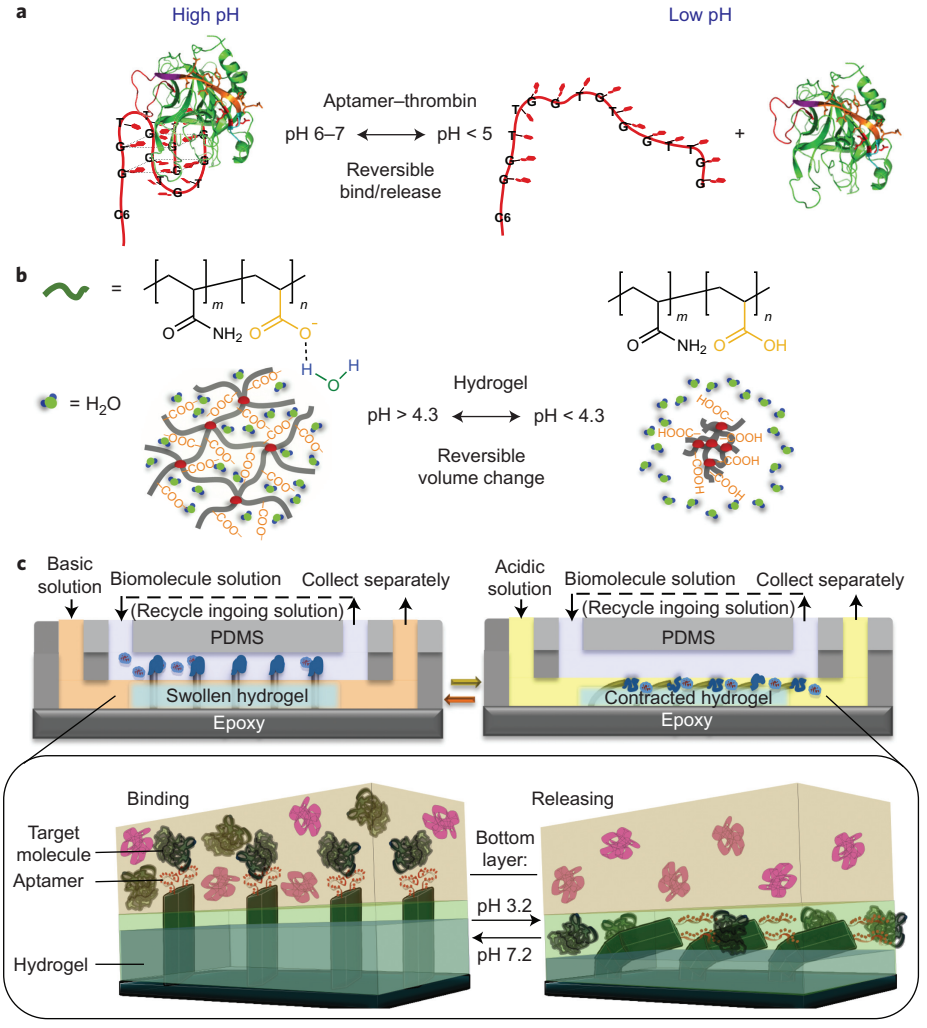

Figure 1 | Design of the chemomechanically modulated biomolecule catch-and-release system. a, pH-dependent reversible binding and releasing of thrombin by the DNA aptamer at pH = 6–7 and pH < 5, respectively, caused by the aptamer configuration change. **b**, pH-dependent reversible volume change of hydrogel (P(AAc-*co*-AAm)), which swells at pH > pK_a = 4.3, when the carboxylic groups are deprotonated, leading to the absorption of water into the gel matrix, and contracts at pH < pK_a = 4.3, which expels water. **c**, Scheme depicting a cross-sectional view of the biphasic microfluidic chamber under constant laminar flow with aptamer-decorated microstructures. The top fluid layer is used to introduce biomolecule mixtures and is kept at physiological pH. In the presence of a solution of pH 7.2, the hydrogel in the bottom layer swells and the aptamer-decorated microfins protrude into the top solution, exposing aptamers to the biomolecule mixture and binding the target biomolecule thrombin in the pH 6.3 buffer. In the presence of an acidic solution, pH 3.2, the hydrogel contracts, which bends the aptamer-decorated microstructures into the bottom layer, resulting in denaturation of the aptamer and release of the captured thrombin molecules. The bottom solution, which contains released target molecules, can be collected separately from the top layer, enabling the separation of target biomolecules from mixtures.

stimulus, such as, for example, pH changes. Aided by computational modelling, we assembled such a system and illustrated its ability to separate an exemplary biomolecule, thrombin, by coordinating the pH-sensitive affinity of the thrombin protein to its aptamer (5′-GGTTGGTGTGGTTGG-3′)[26,27] with the pH-sensitive contraction and expansion of the poly(acrylamide-*co*-acrylic acid) hydrogel (P(AAc-*co*-AAm)). By immersing this hybrid assembly in a microfluidic system under bilayer fluid flow, we achieved the efficient catch of thrombin from the ingoing mixture in the top layer and its subsequent release in the separate flow in the bottom layer. In this way, we exploited the pH-responsive chemomechanobiochemical modulations of the system to separate and collect thrombin from a mixture without the use of expensive and complex tools, which suggests a great promise for point-of-care diagnosis, monitoring, drug testing and sorting for cell-based therapeutics[28–31].

Results and discussion

Design of the chemomechanically modulated system. To enable synchronized hydrogel actuation and target-molecule catch and release in response to a single stimulus, we selected a hydrogel and an aptamer that both respond to changes in pH. We chose a well-characterized aptamer that specifically binds human α-thrombin, 5′-GGTTGGTGTGGTTGG-3′ (a serine protease that plays a key role in the blood-clotting cascade), at an appropriate pH in the range 6–7 (Fig. 1a)[26,27]. Importantly, this aptamer is known to denature reversibly and lose affinity for thrombin at a low pH (Supplementary Fig. 1)[32]. Similarly, P(AAc-*co*-AAm) is a well-studied biocompatible hydrogel that contracts at pH < pK_a = 4.25 and swells at pH > pK_a (Fig. 1b)[17]. We anticipated that linking these two pH-responsive components with flexible epoxy microstructures (10 μm width, 2 μm length, 18 μm height, 5 μm spacing) in a microfluidic system (see Supplementary Fig. 2.1 for

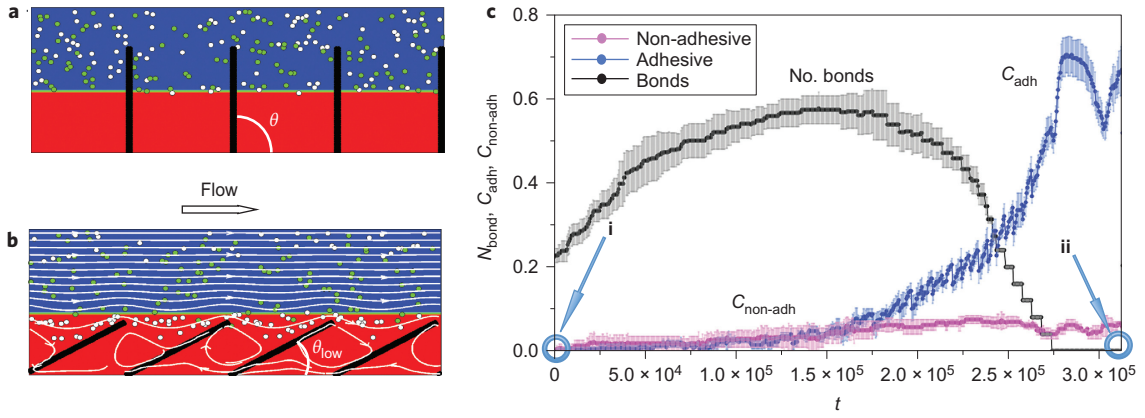

Figure 2 | Computer simulations of the selective binding and release. a,**b**, Snapshots of the system at the onset of simulations at $t = 0$ (**a**) and at later times when the tilt angle between the fins and the bottom substrate is $\theta_{low} = \pi/6$ (**b**). The fins are anchored to the floor of a two-dimensional microchannel and assumed to be actuated by an underlying chemoresponsive gel. After the fins reached the angle θ_{low}, we turned off the fins' motion, but continued to apply the pressure gradient. Adhesive particles are shown in white and non-adhesive particles are shown in green; the total number of particles is $N = 200$ (100 of each type). The fluid streamlines are shown in white. **c**, Evolution of the fraction of particles in the lower stream for adhesive particles, $C_{adh}(t)$ (in blue), and for non-adhesive particles, $C_{non\text{-}adh}(t)$ (in magenta), and the evolution of the number of bonds, N_{bond}, between the fins and the adhesive particles normalized by 100 (in black). The points marked **i** and **ii** on the x axis in **c** correspond to the respective snapshots in **a** and **b**, respectively. For simulation parameters and the relationship between the simulation and experimental values, see Supplementary Section 5.1.

more details) would enable the selective and repetitive capture of active thrombin from a cocktail of molecules flowed into the top layer kept at a constant pH that corresponds to the highest binding efficiency of the aptamer. The target is released and collected in the bottom layer, facilitated by hydrogel volume change-induced microstructure bending, where the pH is alternated between basic and acidic conditions, as schematically presented in Fig. 1c.

To gain insight into the factors that affect the performance of this hybrid system, we first conducted computer simulations of the interactions among the oscillating fins and target proteins, which are modelled as 'adhesive nanoparticles', and non-target proteins, which are simulated as 'non-adhesive particles' (see the Supplementary Information), to identify the conditions in which the selective capture of the target adhesive nanoparticles from the upper mixed fluid stream is followed by their release into the lower stream, which is initially free of particles. To model the actuation, we imposed a periodic motion on the fins, so that the angle θ between a fin and the lower wall varies sinusoidally with time between the values $\theta = \pi/2$ and $\theta = \theta_{low}$ with an angular frequency ω. We focused primarily on the first half of the oscillation cycle, which corresponds to the contraction of the underlying gel. We applied a pressure gradient, ∇P, that drives the fluid from the left to the right along the microchannel and past the oscillating fins, as marked by the arrow in Fig. 2a. We kept the fins stationary after they reached θ_{low}, but continued to apply the pressure gradient. We assumed that the interface between the two fluids remained at a constant position, h_{int}, consistent with previous experimental observations[17,33]. When the fins are tilted at θ_{low}, their tips are below the interface h_{int} (Fig. 2b). Importantly, only the fin sites that are located in the upper phase (above h_{int}) are assumed to be adhesive and able to form strong bonds with the adhesive nanoparticles. The binding between a fin site and a nanoparticle was modelled through a Morse potential, with the binding dependent on the particle–fin separation[34]. These bonds are broken and the respective fin sites become non-adhesive to both types of nanoparticles if they are surrounded by the lower stream.

The simulations show (Fig. 2c) that approximately 70% of the adhesive particles are captured from the upper stream and then released into the lower stream in a given simulation run, whereas less than 10% of the non-adhesive particles are drawn into the lower stream. This is evident from the respective time-evolution curves $C(t)$ (blue and magenta lines in Fig. 2c), which give the ratio between the number of nanoparticles of a given type in the lower phase to the total number of particles of the same type. This selective catch-and-release process can be understood from the evolution of the number of the bonds formed between the adhesive particles and adhesive fin sites (black line in Fig. 2c). The number of bonds formed saturates even when the fins are in the upper fluid, primarily because of the number of available adhesive sites in the system. The number of adhesive sites effectively limits the maximum number of nanoparticles that can potentially be collected in one actuation cycle because each site on a fin can form only a single bond with the adhesive nanoparticle. The simulations clearly demonstrate the feasibility of the proposed synchronized capture and release and selective sorting of the biomolecules.

To realize this system experimentally, the microfluidic channel requires distinct inlets and outlets for the top and bottom layers to maintain an independent control of the pH in each layer and to separate the target molecule from a complex ingoing mixture. The two fluid layers were under constant laminar flow and effectively did not mix within the microfluidic channel or cause microstructure bending by themselves (Supplementary Fig. 2.1). The use of two separate inlets allows for the control of the pH in each layer to create chemically distinct environments for the concerted reconfigurations; the use of two separate outlets provides efficient sorting, without the need for washing steps to remove non-target proteins or separate elution steps to release the captured thrombin. Importantly, the dynamic chemomechanical response of the hydrogel to different pH values in the bottom layer ensures the synchronized removal of the aptamer-bound thrombin from the top layer into the bottom layer with a synchronized chemomechanical reconfiguration in a single step. Moreover, the ability to continuously separate the target molecule from the top layer allows the ingoing solution to be recycled for multiple rounds, which enables separation of nearly all of the target molecules to give a highly efficient biomolecule detection, isolation and purification.

To enable a pH-regulated capture and release, we tested the pH dependence of thrombin–aptamer binding[35,36]. Using an enzyme-linked oligonucleotide immunoassay (ELONA), we observed the highest thrombin–aptamer affinity at pH 6.3 (disassociation constant $K_{d,apparent} \cong 14.8$ nM), and so a buffer of pH 6.3 was used in

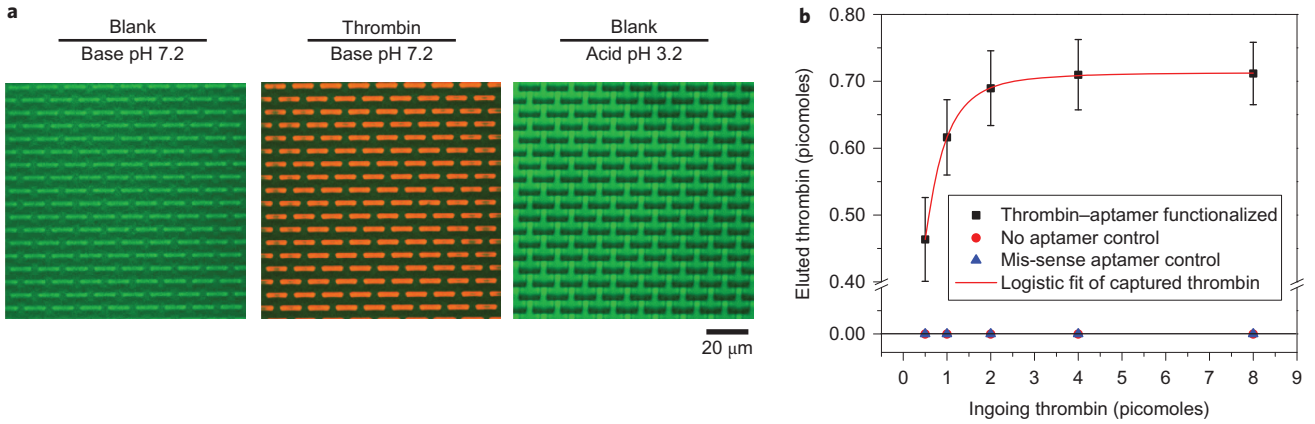

Figure 3 | Chemomechanically modulated sequential catch and release of thrombin in the microfluidic system. a, Top-view confocal microscope images of thrombin capture and release with aptamer-decorated microstructure tips in the biphasic microfluidic system. All the images focus on microstructure tips and are composites of two wavelengths, 488 nm (to visualize autofluorescence of the epoxy microstructures) and 543 nm (to visualize Dylight dye-labelled thrombin). Left image: microstructures stand upright when a basic buffer (pH 7.2) flows through the bottom layer; when a blank solution that contains no thrombin is flowed in the top layer, only epoxy autofluorescence is detected. Middle image: when the hydrogel is swollen in a basic buffer (pH 7.2), dye-labelled thrombin is flowed through the top layer and is captured by aptamers on the microstructure tips standing upright. Right image: introducing acidic buffer (pH 3.2) into the bottom layer bends the microstructures into the bottom layer and releases dye-labelled thrombin from the aptamer-decorated microstructure tips, whereas the blank solution flows in the top layer. **b**, Sorting capacity of the microfluidic system. Increasing quantities of thrombin are pumped into the top layer of the microfluidic channel (dimensions 0.5 mm × 8 mm × 0.06 mm). After microstructure bending, the bottom layer solution is collected and the eluted thrombin is quantified by ELISA. The amount of captured thrombin saturates at 0.71 picomoles, which defines the sorting capacity. Error bars = standard deviation, $n = 4$.

the top layer, in which the aptamer–thrombin binding occurs (Supplementary Fig. 1). A buffer with pH 7.2 was used in the bottom layer to swell the hydrogel and straighten the microstructures so that the aptamer-bearing tips would protrude into the top fluid for binding. Once thrombin is captured by the aptamer in the top layer, the release of the target into the bottom layer will occur at a pH that permits both a fast and sufficient hydrogel contraction and an aptamer reconfiguration to decrease the binding to thrombin. An ELONA showed a substantial reduction in the aptamer–thrombin affinity on decreasing the pH from pH 6.3 to pH 5.0 ($K_{d,apparent} = 35$ nM) (Supplementary Fig. 1). The onset of hydrogel contraction is at pH 4.3, so we chose a buffer with pH 3.2 for use in the bottom layer to ensure both a sufficient bending of the microstructures and a sufficient dissociation of the bound thrombin, as depicted in Fig. 1c.

Decoration of the epoxy microfin tips with a DNA aptamer was verified by X-ray photoelectron spectroscopy (XPS) (Supplementary Fig. 2.2b) and confocal microscopy, which detected fluorescence that corresponds to a modified DNA strand complementary to the aptamer on the tips of the functionalized microfins, but not on the control microfins (Supplementary Fig. 2.2). Fluorescently labelled thrombin was then flowed through the microfluidic channel and subjected to one cycle of capture (bottom layer pH = 7.2), transport and release (bottom layer pH = 3.2). Confocal microscopy demonstrated that thrombin was bound to the tips of the microfins when the bottom layer solution was at pH 7.2 and was absent after this bottom layer was replaced with a solution of pH 3.2 (Fig. 3a). In a control experiment, the fluorescence of the thrombin label remained unaffected by switching the pH from 6.3 to 3.2 (Supplementary Fig. 3.1), which thus validates the successful release of thrombin at pH 3.2. Importantly, the released thrombin retained an antibody-binding activity comparable to that of untreated thrombin (Supplementary Fig. 3.2). Computational simulation also showed that the fluid continues to flow along the channel above the bent fins for a smooth protein release and movement to the collection outlet (see Supplementary Fig. 8). These results demonstrate that the microsystem enables the concerted, non-destructive catch–transport–release of a target biomolecule, with the collected biomolecules remaining active and suitable for further use and analysis.

Evaluation of the system's catch-and-release capability. To study and systematically quantify the total binding capacity of the biomolecule sorting, as well as its effectiveness in capturing the target molecule, we injected into the device solutions of the same volume but with increasing concentrations of thrombin (translating into 0.5, 1.0, 2.0, 4.0 and 8.0 picomoles total thrombin), then proceeded through the release step, and collected and analysed the bottom layer of the outgoing solutions. The collected amount of thrombin increased with the increase in the injected amount and eventually levelled off to form a plateau at ~0.7 picomoles for 4.0 and 8.0 picomoles ingoing thrombin (Fig. 3b). This value represents the maximum binding capacity of the microfluidic sorting system with the given flow characteristics, dimensions of the channel and specific microfin area (0.5 × 8 mm) both available for the aptamer functionalization and exposed to the top layer. Although there is a clear plateau, the error in these measurements represents experiments conducted with four different microdevices with the same dimensions and volume, in which the differences could arise from aptamer functionalization and the measurement of thrombin with enzyme-linked immunosorbent assay (ELISA). This finite capacity correlates well with the simulations shown in Fig. 2, which suggest that no additional capture occurs when all the adhesive sites are saturated. The sorting efficiency of the system can be defined, therefore, as the amount of target molecule captured, transported and released in one actuation cycle relative to the dimension- and flow-determined maximum binding capacity of the system (0.7 picomoles in the current set-up) for various ingoing biomolecule concentrations (see Methods for details). Importantly, the same experiments with either no aptamer on the fins or a scrambled sequence in place of the aptamer did not produce detectable levels of thrombin in the bottom effluent layer (Fig. 3b). Taken together, these results prove the ability of our system to capture and release the target biomolecule from ingoing solutions with a broad range of concentrations. Furthermore, they

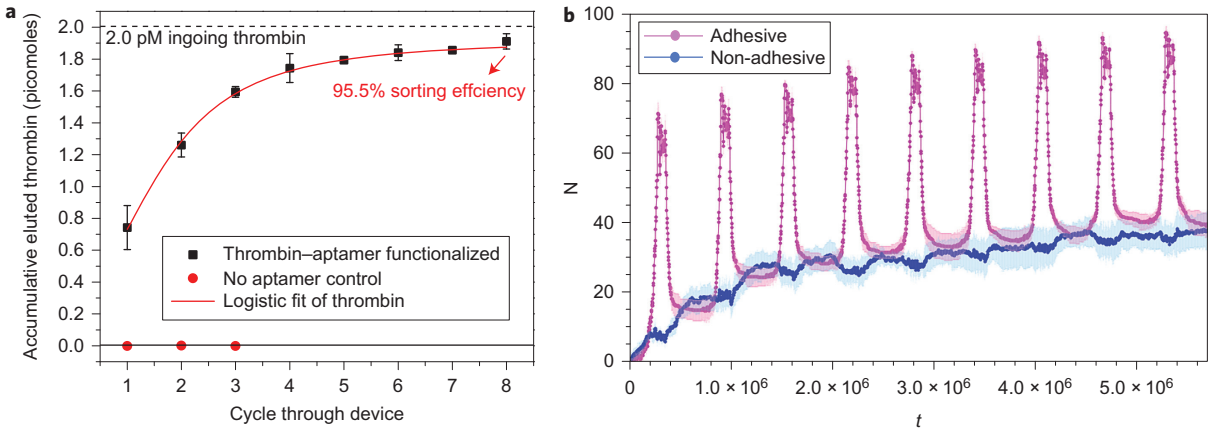

Figure 4 | System performance in multiple oscillation cycles with recycling of the ingoing solution. a, Thrombin collected from recycling of the ingoing solution. Thrombin (2 picomoles) was pumped into the top layer of the microfluidic channel. After each actuation of the system, the bottom solution was collected and the top layer was recycled through the channel. Eluted thrombin was quantified by ELISA. The cumulative amount of eluted thrombin after each actuation was calculated and plotted. The control system that contained no aptamer shows no measurable elution of thrombin; the aptamer-functionalized system shows elution of 95.5% of the ingoing thrombin in the bottom layer after eight cycles of capture and release. The near-quantitative recovery of the ingoing thrombin suggests that the surfaces of the microfluidic channel and the hydrogel have very little non-specific association with the target protein. **b**, Computer simulations that show the evolution of the number of particles in the lower stream, *N*, for adhesive nanoparticles (in magenta) and non-adhesive nanoparticles (in blue) for a total of 200 particles (100 of each type) during nine oscillation cycles.

demonstrate the robustness of the integrated chemistries of binding and release and their compatibility with the hydrodynamic and/or diffusion characteristics of the microfluidic sorting system.

Most analytical applications require high levels of analyte separation and the ability to reuse the device multiple times. We anticipated that recycling the ingoing solution in our system would allow for the recovery of thrombin that was not captured in the previous cycles. Indeed, when a solution initially containing 2 picomoles thrombin was introduced and recycled eight times through the microfluidic channel, the amount of recovered thrombin grew from ~0.7 picomoles after the first cycle to ~1.9 picomoles, thus reaching nearly 95.5% of the total ingoing thrombin (Fig. 4a). This clearly demonstrates the system's robustness and efficacy in repeated catch–transport–release cycles.

Multiple actuation cycles were also examined in the computer simulations to probe the capture–transport–release dynamics associated with the repeated oscillations of the fins. Here the peak values correspond to the microstructures bent into the lower phase when the fraction of adhesive particles in the lower phase was maximized. Qualitatively similar to the experiments, this peak value, or the fraction of particles removed from the upper into the lower stream, increased during each cycle. These simulations illustrate that the catch-and-release effect is robust even in 'harsher' conditions in which a portion of the adhesive nanoparticles is continuously brought back into the upper stream during the recovery stroke. In contrast, in the experimental device, released proteins flow through the lower stream outlet port. However, similar to the experiments, in the simulations about 95% of the adhesive nanoparticles had been released into the lower phase by the ninth cycle (Fig. 4b) and this number continued to increase in subsequent cycles. This indicates that the catch-and-release system can be expected to work in a qualitatively similar manner for a wide range of recycling conditions.

To test experimentally the system's ability to capture thrombin selectively from a mixture of proteins, a solution that contained a mixture of thrombin and transferrin, an iron-binding plasma glycoprotein, and a mixture of thrombin and bovine serum albumin (BSA) were introduced into the microfluidic channel with aptamer-decorated and unfunctionalized microstructures, as well as microstructures functionalized with a scrambled DNA sequence that does not bind thrombin[32,37]. The resulting top and bottom fluids were collected separately and analysed by polyacrylamide gel electrophoresis (PAGE). The thrombin aptamer-decorated system selectively captured thrombin from the top fluid and released it in the bottom solution for both mixtures, with both BSA and transferrin retained in the top layer; additionally, all the thrombin, transferrin and BSA were retained in the top layer in the control systems (Fig. 5a,b). To further test the efficacy of filtrating a specific protein from a more-complex blood-like environment, human serum that contained thrombin was introduced into the system in a similar way with the thrombin successfully separated out (Fig. 5c and Supplementary Fig. 4), which confirms the design's generality and applicability to sorting biomolecules from mixtures. It is evident that there is very little non-specific interaction of the device with the solution mixture, because non-specific fouling is reduced by the constant flow of biomolecules through the device.

Each component of our chemomechanically modulated system can be tailored individually to produce the desired output. For example, the hydrogel composition, microstructure material, geometry and array dimensions, and functionalization of the microstructure tips can all be adjusted. As one example, the hydrogel composition can be changed to alter its response time or its degree of swelling (and, correspondingly, the tilt angle of the microfins, θ_{low}). With the aid of the computer simulations, we can predict the influence of these parameters on the system's performance. For instance, we show that for a given interface height, there is a well-defined range of θ_{low} values that results in an efficient catch and release; however, an increase in θ_{low} above the threshold value results in a rapid decrease in the fraction of adhesive particles released into the lower stream (Supplementary Fig. 6). We found the system's performance to be relatively insensitive to τ_{down} (Supplementary Fig. 7). Finally, our simulations show that varying the position of the fluid–fluid interface can also be used to adjust the system's efficiency and indicate an optimal interface height for a given fin length (see Supplementary Section 5.2.1).

Conclusions

We have designed and tested a miniature bioinspired microfluidic system that uniquely couples pH-manipulated microfin actuation with pH-dependent aptamer unfolding and refolding for

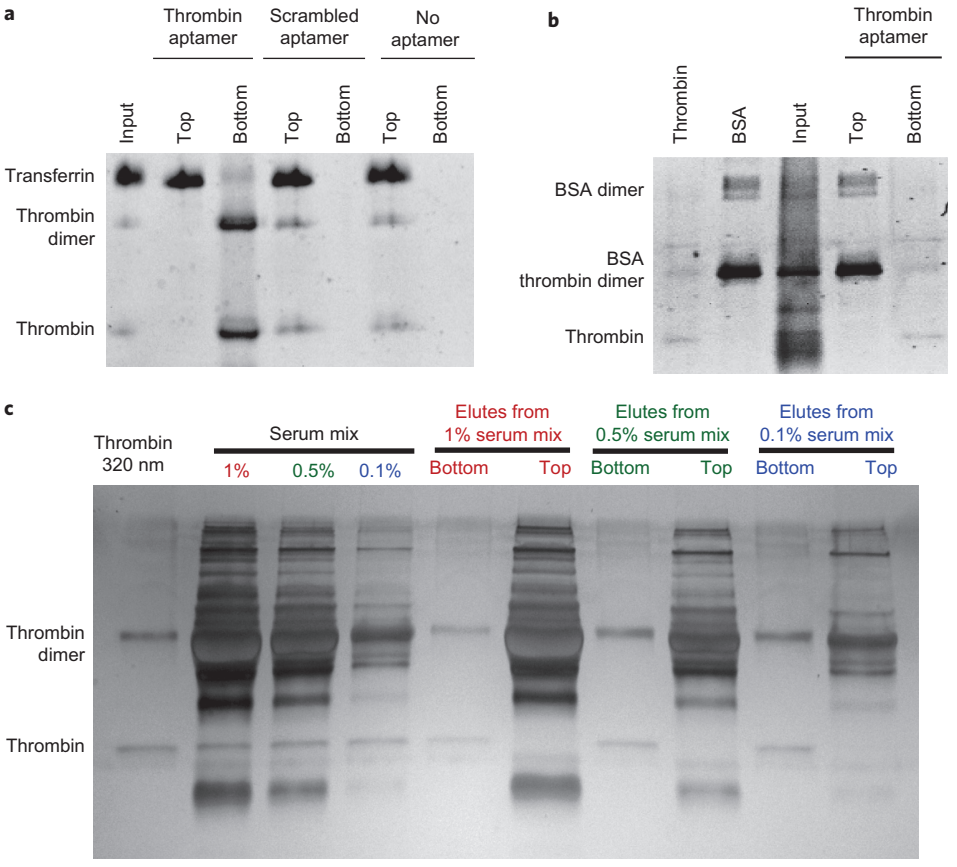

Figure 5 | Analysis of the components of the top and bottom solutions after cycling. a–c, A solution of thrombin mixed with different interfering non-target protein(s), including transferrin (**a**), BSA (**b**) and 1, 0.5 and 0.1% human serum (**c**), was pumped into the top layer of the microsystem. The top layer was recycled multiple times through the channel over repeated hydrogel actuations and was collected after the final actuation, whereas solutions from the bottom layer were collected after each actuation and pooled for PAGE analysis. In a microsystem functionalized with a thrombin aptamer, thrombin was eluted specifically from the bottom layer, whereas the interfering non-target protein(s), that is, transferrin, BSA and other proteins in the serum, were retained in the top layer, despite repeated cycling of the top-layer solution. In **a**, in control experiments in which the microstructures were either unfunctionalized or decorated with a non-binding scrambled DNA sequence, both thrombin and transferrin were retained in the top layer.

biomolecule catch–transport–release, and offers the non-destructive separation of specific molecules from a complex solution through a robust and tunable chemomechanobiochemical process. Additionally, the reversibility of hydrogel swelling and aptamer folding allows the repeated processing of a single input solution, which enables multiple recycling and a high capture of the target molecules from the initial mixture. Compared to other small-volume biomolecule-sorting systems that rely on external electric fields[38], infrared radiation[39] and magnetic fields[7,40], and require chemical modifications of the biomolecules of interest[41], which leads to the once-only use of a given set-up[42] or requires a series of sequential steps for the release of the biomolecule and/or reuse of the device[32,43], our system can exploit coupled chemistries in a microfluidic channel to yield both efficient (minimal steps) and effective (recovery of almost all of the target biomolecule from solution) output.

The reversible chemomechanical modulation character of this system makes it suitable for numerous applications that require the separation of microlitre samples for downstream analysis with a low turnaround time. The variability and tunability of the hydrogel, aptamer-binding strength, geometry and material of the microstructure, and flow characteristics make this system a broad-based, customizable platform for multiple applications. The microstructures can be functionalized with a diverse array of environmentally responsive aptamers, antibodies, catalysts or small molecules, and in principle allows the attachment of several target molecules. SELEX (systematic evolution of ligands by exponential enrichment) allows the easy identification of aptamer sequences that can target a broad range of proteins and molecules under a variety of conditions, and so enables the selection of a binding that is responsive to factors such as pH, temperature, salt and so on.[44–46]. As research on aptamers expands and the modification of aptamers with appropriate ionizable groups becomes increasingly viable[47,48] for pH-dependent behaviour, our platform can also be used for such targets. In addition, G-quartet binding, which is involved in the aptamer–thrombin binding in this work, is evident in many other sequence–target configurations, which probably also makes our proof-of-concept applicable to these other biomolecules[49,50]. The chemistry of the hydrogel can be tuned to achieve stimuli-responsive sorting at various conditions, as hydrogels can be made to respond to temperature, light, electric and/or magnetic fields, ionic concentration and so on. Such a broad spectrum of multiple chemistries possible within a single, dynamic system could find further applications not only in biomedical fields, but also in the fields of inorganic and/or synthetic chemistry for the microfluidic analysis of chemical binding/releasing and sensing to determine chemical purity, chirality, molecular binding kinetics or affinity in different environments.

Methods

Chemicals. Acrylamide (AAm), acrylic acid (AAc), dodecyl acrylate, glycidyl methacrylate, 2-hydroxy-4′-(2-hydroxyethoxy)-2-methylpropiophenone (Irgacure

2959, photoinitiator), (tridecafluoro-1,1,2,2-tetrahydrooctyl)trichlorosilane and dithiothreitol (DDT) were purchased from Sigma-Aldrich and used as received. Polydimethylsiloxane (PDMS) (Dow-Sylgard 184) was purchased from Ellsworth and UVO-114 was purchased from Epoxy Technology. For ELONA measurements, clear streptavidin-coated 96-well plates were obtained from Thermo Scientific. The antithrombin horseradish peroxidase polyclonal antibody conjugate for the ELONA assays was purchased from Thermo Scientific. A solution of 3,3′,5,5′-tetramethylbenzidine (TMB) with hydrogen peroxide was purchased from Thermo Scientific. For thrombin detection, a thrombin-specific ELISA kit was purchased from Antibodies-online.com. Human plasma thrombin was purchased from EMD Millipore Chemicals. Human transferrin (98%) and human serum from human male AB plasma were purchased from Sigma-Aldrich.

DNA synthesis. Oligonucleotides were purchased from Integrated DNA Technologies or synthesized on a PerSeptive Biosystems Expedite 8909 DNA synthesizer using reagents and phosphoramidites purchased from Glen Research. Oligonucleotides were synthesized and deprotected according to the manufacturer's protocols and purified by either an oligonucleotide purification cartridge (ABI) or by reverse-phase high-pressure liquid chromatography (HPLC, Agilent 1200) using a C18 stationary phase and an acetonitrile/100 mM trimethylammonium acetate gradient. Non-commercial oligonucleotides were characterized by liquid chromatography/electrospray-ionization mass spectrometry with reverse-phase separation on an Alliance 2695 (Waters) HPLC system using a UPLC BEH C18 column (1.7 μM, 2.1 × 50 mm) stationary phase and a 6 mM aqueous triethylammonium bicarbonate/methanol mobile phase interfaced to a Micromass Q-ToF Micro mass spectrometer (Waters). The thrombin aptamer was 5′-GGTTGGTGTGGTTGG-thiol C6 SS-3′ synthesized using a 3′ thiol C6-modified controlled pore glass resin (Glen Research). The biotinylated thrombin aptamer was 5′-GGTTGGTGTGGTTGG-biotinTEG-3′ synthesized using a 3′ biotinTEG resin (Glen Research). The scrambled thrombin aptamer was 5′-GGTGGTGGTTGTGGT-thiol C6 SS-3′. The thrombin aptamer probe was 5′-/5Cy5/ CCA ACC ACA CCA ACC -3′.

Deprotection of the aptamer disulfide to free thiol. Purified DNA aptamers were diluted in phosphate-buffered saline (pH 7.2) and combined with 0.1 volumes 1 M DTT (Sigma-Aldrich). This mixture was incubated at room temperature for 30 minutes before the free 3′-thiol linked aptamer was recovered by ethanol precipitation.

Functionalization of the microstructure tips with the aptamer. A PDMS block was used to stamp 3′-thiol-modified aptamers onto the epoxy microfins. An aptamer solution (20 μl, 10 mM) was applied to a small area of PDMS, which was then carefully placed on top of the oxygen-plasma-treated epoxy structures and left to incubate overnight at 4 °C. Thorough washing of the sample removed excess unbound aptamer from the microstructured sample.

Biomolecule sorting and collection in the microfluidic system. BSA blocking solution (100 μl, 500 nM) was flowed through the channel. Subsequently, 100 μl of thrombin solution in a pH 6.3 buffer was flowed into the top layer at the same times as 100 μl of a pH 7.2 buffer was flowed into the bottom layer. To determine the sorting capacity of the microfluidic system, 100 μl of different initial thrombin concentrations, 5 nM, 10 nM, 20 nM, 40 nM and 80 nM, were flowed into the top layer. The outgoing solution (100 μl) was collected from the top layer. The flow rate was 10 μl min^{-1} for the top fluid and 30 μl min^{-1} for the bottom fluid. For biomolecule release, 100 μl of a pH 6.3 buffer that contained no biomolecules was flowed into the top layer and 100 μl of a pH 3.2 buffer was flowed into the bottom layer to contract the hydrogel and release bound biomolecules. The outgoing solution (100 μl) was collected from the bottom layer. The collected aliquots were diluted and analysed with ELISA (described below). To determine the sorting ability with multiple sorting cycles of a given thrombin solution, the process described was repeated eight times whereby the same initial ingoing thrombin solution in the first cycle was reintroduced through the top layer at each subsequent cycle.

PAGE experiment for selectivity test. Fractions from the top and bottom layers of the channel were collected and pooled after several actuations had been conducted on an ingoing mixture solution containing 20 nM thrombin and 20 nM transferrin, 20 nM BSA or 1, 0.5 or 0.1% human serum. The top-layer eluting solutions were repumped in the microsystem multiple times, eight times for transferrin- and BSA-containing mixture and 40, 20 and 10 times for 1, 0.5 and 0.1% serum mixtures, respectively. Fractions were concentrated by lyophilization, redissolved in a 1× NuPAGE protein-loading buffer (Invitrogen), heated to 95 °C for five minutes and analysed by electrophoresis (12% NuPAGE gel (Invitrogen), 200 V, 45 minutes) The gel was subsequently stained with Sypro Ruby (Sigma) and imaged on a ChemiImager.

ELISA experiment for the quantitative measurement of thrombin concentration. To measure the amount of thrombin eluted from the top and bottom layers of the microfluidic channel, a thrombin-specific ELISA kit (Fisher Scientific) was used. Standard curves were made of thrombin at known concentrations in the relevant pH buffers, pH 6.3 and pH 3.2. Aliquots of the collected solutions from the top and bottom layers were diluted appropriately and dispensed, along with the standard solutions, onto a microplate precoated with a monoclonal antibody specific for thrombin. After incubation of the thrombin solutions for two hours, the unbound thrombin was washed away. A biotinylated polyclonal thrombin antibody was then incubated on the microplate for one hour. After washing away excess unbound antithrombin, streptavidin peroxidase conjugate was deposited onto the microplate to recognize the bound antithrombin antibody and left to incubate for 30 minutes. After washing away excess streptavidin peroxidase conjugate, a chromogenic substrate, TMB, was added to the microplate and incubated for ten minutes, after which 0.5 N HCl solution was added to stop the chromogen substrate reaction and the absorbance was quantified at 450 nm. The intensity of absorption at 450 nm for the collected thrombin was compared to a standard curve to calculate the amount of collected thrombin on the SpectraMax M5 from Molecular Devices.

Received 30 October 2014; accepted 12 February 2015; published online 23 March 2015

References

1. Fratzl, P. & Barth, F. G. Biomaterial systems for mechanosensing and actuation. *Nature* **462,** 442–448 (2009).
2. Stuart, M. A. C. *et al.* Emerging applications of stimuli-responsive polymer materials. *Nature Mater.* **9,** 101–113 (2010).
3. Cabodi, M., Chen, Y. F., Turner, S. W. P., Craighead, H. G. & Austin, R. H. Continuous separation of biomolecules by the laterally asymmetric diffusion array with out-of-plane sample injection. *Electrophoresis* **23,** 3496–3503 (2002).
4. Cho, E. J., Collett, J. R., Szafranska, A. E. & Ellington, A. D. Optimization of aptamer microarray technology for multiple protein targets. *Anal. Chim. Acta* **564,** 82–90 (2006).
5. Eigen, M. & Rigler, R. Sorting single molecules—application to diagnostics and evolutionary biotechnology. *Proc. Natl Acad. Sci. USA* **91,** 5740–5747 (1994).
6. Song, Y. A., Hsu, S., Stevens, A. L. & Han, J. Y. Continuous-flow pI-based sorting of proteins and peptides in a microfluidic chip using diffusion potential. *Anal. Chem.* **78,** 3528–3536 (2006).
7. Fu, J., Mao, P. & Han, J. Artificial molecular sieves and filters: a new paradigm for biomolecule separation. *Trends Biotechnol.* **26,** 311–320 (2008).
8. He, X., Li, C., Chen, F. G. & Shi, G. Q. Polypyrrole microtubule actuators for seizing and transferring microparticles. *Adv. Funct. Mater.* **17,** 2911–2917 (2007).
9. Zhao, Q., Li, X-F. & Le, X. C. Aptamer capturing of enzymes on magnetic beads to enhance assay specificity and sensitivity. *Anal. Chem.* **83,** 9234–9236 (2011).
10. Levy-Nissenbaum, E., Radovic-Moreno, A. F., Wang, A. Z., Langer, R. & Farokhzad, O. C. Nanotechnology and aptamers: applications in drug delivery. *Trends Biotechnol.* **26,** 442–449 (2008).
11. Sengupta, S. *et al.* Self-powered enzyme micropumps. *Nature Chem.* **6,** 415–422 (2014).
12. Koga, S., Williams, D. S., Perriman, A. W. & Mann, S. Peptide–nucleotide microdroplets as a step towards a membrane-free protocell model. *Nature Chem.* **3,** 720–724 (2011).
13. Maitz, M. F. *et al.* Bio-responsive polymer hydrogels homeostatically regulate blood coagulation. *Nature Commun.* **4,** 2168 (2013).
14. Rodriguez-Llansola, F. & Meijer, E. W. Supramolecular autoregulation. *J. Am. Chem. Soc.* **135,** 6549–6553 (2013).
15. Wang, J. B. & Feringa, B. L. Dynamic control of chiral space in a catalytic asymmetric reaction using a molecular motor. *Science* **331,** 1429–1432 (2011).
16. Wilson, D. A., Nolte, R. J. M. & van Hest, J. C. M. Autonomous movement of platinum-loaded stomatocytes. *Nature Chem.* **4,** 268–274 (2012).
17. He, X. *et al.* Synthetic homeostatic materials displaying chemo-mechano-chemical self-regulation. *Nature* **487,** 214–218 (2012).
18. de Ruiter, G. & van der Boom, M. E. Surface-confined assemblies and polymers for molecular logic. *Acc. Chem. Res.* **44,** 563–573 (2011).
19. Krieg, E., Weissman, H., Shirman, E., Shimoni, E. & Rybtchinski, B. A recyclable supramolecular membrane for size-selective separation of nanoparticles. *Nature Nanotech.* **6,** 141–146 (2011).
20. Hirokawa, N. Kinesin and dynein superfamily proteins and the mechanism of organelle transport. *Science* **279,** 519–526 (1998).
21. Cho, E. J., Lee, J. W. & Ellington, A. D. Applications of aptamers as sensors. *Ann. Rev. Anal. Chem.* **2,** 241–264 (2009).
22. Mosing, R. K. & Bowser, M. T. Microfluidic selection and applications of aptamers. *J. Sep. Sci.* **30,** 1420–1426 (2007).
23. Jeong, B. & Gutowska, A. Lessons from nature: stimuli-responsive polymers and their biomedical applications. *Trends Biotechnol.* **20,** 305–311 (2002).
24. Yerushalmi, R., Scherz, A., van der Boom, M. E. & Kraatz, H. B. Stimuli responsive materials: new avenues toward smart organic devices. *J. Mater. Chem.* **15,** 4480–4487 (2005).
25. Krieg, E. *et al.* Supramolecular gel based on a perylene diimide dye: multiple stimuli responsiveness, robustness, and photofunction. *J. Am. Chem. Soc.* **131,** 14365–14373 (2009).
26. Macaya, R. F., Schultze, P., Smith, F. W., Roe, J. A. & Feigon, J. Thrombin-binding DNA aptamer forms a unimolecular quadruplex structure in solution. *Proc. Natl Acad. Sci. USA* **90,** 3745–3749 (1993).

27. Tasset, D. M., Kubik, M. F. & Steiner, W. Oligonucleotide inhibitors of human thrombin that bind distinct epitopes. *J. Mol. Biol.* **272,** 688–698 (1997).
28. Srinivas, R. L., Chapin S. C. & Doyle, P. S. Aptamer-functionalized microgel particles for protein detection. *Anal. Chem.* **83,** 9138–9145 (2011).
29. Cheng, M. M. C. *et al*. Nanotechnologies for biomolecular detection and medical diagnostics. *Curr. Opin. Chem. Biol.* **10,** 11–19 (2006).
30. Guo, M. T., Rotem, A., Heyman, J. A. & Weitz, D. A. Droplet microfluidics for high-throughput biological assays. *Lab Chip* **12,** 2146–2155 (2012).
31. Martinez, A. W., Phillips, S. T., Whitesides, G. M. & Carrilho, E. Diagnostics for the developing world: microfluidic paper-based analytical devices. *Anal. Chem.* **82,** 3–10 (2010).
32. Dick, L. W. & McGown, L. B. Aptamer-enhanced laser desorption/ionization for affinity mass spectrometry. *Anal. Chem.* **76,** 3037–3041 (2004).
33. He, X., Friedlander, R. S., Zarzar, L. D. & Aizenberg, J. Chemo-mechanically regulated oscillation of an enzymatic reaction. *Chem. Mater.* **25,** 521–523 (2013).
34. Bhattacharya, A. & Balazs, A. C. Stiffness-modulated motion of soft microscopic particles over active adhesive cilia. *Soft Matter* **9,** 3945–3955 (2013).
35. Hianik, T. O. V., Sonlajtnerova, M. & Grman, I. Influence of ionic strength, pH and aptamer configuration for binding affinity to thrombin. *Bioelectrochemistry* **70,** 127–133 (2007).
36. Baldrich, E., Restrepo, A. & O'Sullivan, C. K. Aptasensor development: elucidation of critical parameters for optimal aptamer performance. *Anal. Chem.* **76,** 7053–7063 (2004).
37. Bock, L. C., Griffin, L. C., Latham, J. A., Vermaas, E. H. & Toole, J. J. Selection of single-stranded DNA molecules that bind and inhibit human thrombin. *Nature* **355,** 564–566 (1002).
38. Zeng, Y. & Harrison, D. J. Self-assembled colloidal arrays as three-dimensional nanofluidic sieves for separation of biomolecules on microchips. *Anal. Chem.* **79,** 2289–2295 (2007).
39. Arakawa, T., Shirasaki, Y., Aoki, T., Funatsu, T. & Shoji, S. Three-dimensional sheath flow sorting microsystem using thermosensitive hydrogel. *Sensor Actuator A* **135,** 99–105 (2007).
40. Doyle, P. S., Bibette, J., Bancaud, A. & Viovy, J. L. Self-assembled magnetic matrices for DNA separation chips. *Science* **295,** 2237–2237 (2002).
41. Pedersen, J., Petersen, G. E., Lauritzen, C. & Arnau, J. Current strategies for the use of affinity tags and tag removal for the purification of recombinant proteins. *Protein Expres. Purif.* **48,** 1–13 (2006).
42. Chen, L. *et al*. Aptamer-mediated efficient capture and release of T lymphocytes on nanostructured surfaces. *Adv. Mater.* **23,** 4376–4380 (2011).
43. Zhang, L., Chatterjee, A. & Leung, K. T. Hydrogen-bond-mediated biomolecular trapping: reversible catch-and-release process of common biomolecules on a glycine-functionalized Si(111)7×7 Surface. *J. Phys. Chem. Lett.* **1,** 3385–3390 (2010).
44. Jayasena, S. D. Aptamers: an emerging class of molecules that rival antibodies in diagnostics. *Clin. Chem.* **45,** 1628–1650 (1999).
45. Wochner, A. *et al*. A DNA aptamer with high affinity and specificity for therapeutic anthracyclines. *Anal. Biochem.* **373,** 34–42 (2008).
46. Zhai, G., Iskander, M., Barilla, K. & Romaniuk, P. J. Characterization of RNA aptamer binding by the Wilms' tumor suppressor protein WT1. *Biochemistry* **40,** 2032–2040 (2001).
47. Lin, Y., Qiu, Q., Gill, S. C. & Jayasena, S. D. Modified RNA sequence pools for *in vitro* selection. *Nucleic Acids Res.* **22,** 5229–5234 (1994).
48. Schurer, H. *et al*. Aptamers that bind to antibiotic moenomycin A. *Bioorg. Med. Chem.* **9,** 2557–2563 (2001).
49. Li, T., Shi, L., Wang, E. & Dong, S. Multifunctional G-quadruplex aptamers and their applications to protein detection. *Chem. Eur. J.* **15,** 1036–1042 (2009).
50. Fujita, H. *et al*. Structural and affinity analyses of G-quadruplex DNA aptamers for camptothecin derivatives. *Pharmaceuticals* **6,** 1082–1093 (2013).

Acknowledgements

This work was supported by the Department of Energy under Award No. DE-SC0005247. We thank M. Krogsgaard and C. Howell for their help with the XPS characterization of the aptamer functionalization of the microstructures.

Author contributions

X.H., A.S., L.M.M., M.A., A.C.B. and J.A. designed the project. X.H., A.S., L.M.M., M.A., O.K., A.C.B. and J.A. wrote the manuscript. Y.L., A.B., Y.M., O.K. and A.C.B. performed the computational simulations and analysed the results. L.M.M. and V.H. performed the PAGE experiments and analysis, and participated in synthesizing the DNA aptamers. X.H. and A.S. conducted the catch-and-release experiments in the microfluidic system and performed the ELISA analysis. X.H., A.S., H.N., M.M. and V.H. conducted the ELONA experiments. A.S. performed the experiments to determine the pH-dependent behaviour of the aptamers. X.H. performed a confocal microscopy characterization of the system. Y.V., O.K. and M.A. contributed important discussions to the analysis of the results.

Additional information

Supplementary information is available in the online version of the paper. Reprints and permissions information is available online at www.nature.com/reprints. Correspondence and requests for materials should be addressed to J.A. and X.H.

Competing financial interests

The authors declare no competing financial interests.